# Radiative Heating and the Buoyant Rise of Magnetic Flux Tubes in the Solar Interior

Y. Fan
National Solar Observatory†, 950 N. Cherry Ave., Tucson, AZ 85719.

G. H. Fisher
Space Sciences Laboratory, Univ. of California, Berkeley, CA 94720-7450

(*accepted by Solar Physics*)

† The National Solar Observatory is one of the National Optical Astronomy Observatories operated by the Association of Universities for Research in Astronomy, Inc., under cooperative agreement with the National Science Foundation.

## Abstract

We study the effect of radiative heating on the evolution of thin magnetic flux tubes in the solar interior and on the eruption of magnetic flux loops to the surface. Magnetic flux tubes experience radiative heating because 1) the mean temperature gradient in the lower convection zone and the overshoot region deviates substantially from that of radiative equilibrium, and hence there is a non-zero divergence of radiative heat flux; and 2) The magnetic pressure of the flux tube causes a small change of the thermodynamic properties within the tube relative to the surrounding field free fluid, resulting in an additional divergence of radiative heat flux. Our calculations show that the former constitutes the dominant source of radiative heating experienced by the flux tube.

In the overshoot region, the radiative heating is found to cause a quasi-static rising of the toroidal flux tubes with an upward drift velocity $\sim 10^{-3}|\delta|^{-1}$ cm s$^{-1}$, where $\delta \equiv \nabla - \nabla_{\rm ad} < 0$ describes the subadiabaticity in the overshoot layer. The upward drift velocity does not depend sensitively on the field strength of the flux tubes. Thus in order to store toroidal flux tubes in the overshoot region for a period comparable to the length of the solar cycle, the magnitude of the subadiabaticity $\delta$ ($< 0$) in the overshoot region must be as large as $\sim 3 \times 10^{-4}$. We discuss the possibilities for increasing the magnitude of $\delta$ and for reducing the rate of radiative heating of the flux tubes in the overshoot region.

Using numerical simulations we study the formation of "$\Omega$" shaped emerging loops from toroidal flux tubes in the overshoot region as a result of radiative heating. The initial toroidal tube is assumed to be non-uniform in its thermodynamic properties along the tube and lies at varying depths beneath the base of the convection zone. The tube is initially in a state of neutral buoyancy with the internal density of the tube plasma equal to the local external density. We find from our numerical simulations that such a toroidal tube rises quasi-statically due to radiative heating. The top portion of the non-uniform tube first enters the convection zone and may be brought to an unstable configuration which eventually leads to the eruption of an anchored flux loop to the surface. Assuming reasonable initial parameters, our numerical calculations yield fairly short rise times (2-4 months) for the development of the emerging flux loops. This suggests that radiative heating is an effective way of causing the eruption of magnetic flux loops, leading to the formation of active regions at the surface.

## 1. Introduction

Active regions at the solar surface are believed to form through the emergence of "Ω" shaped loops of magnetic flux from the base of the convection zone where the solar cycle dynamo operates. Using the dynamic model of thin magnetic flux tubes described by Spruit 1981, numerical simulations have been carried out to study the buoyant rise of magnetic flux tubes through the convection zone (e.g. Choudhuri 1989; D'Silva & Choudhuri 1993; Fan, Fisher, & McClymont 1994; Caligari, Moreno-Insertis, & Schüssler 1995 ). Nearly all of the existing simulations have assumed adiabatic evolution of the flux tubes. The main difference between these simulations is the initial thermodynamic states of the toroidal tubes used. Moreno-Insertis, Schüssler, & Ferris-Mas (1992) and Ferris-Mas & Schüssler (1994) have argued that the most natural initial state for a toroidal flux tube stored in the stable overshoot region is that of neutral buoyancy, where the density of the tube plasma is equal to the external density. Caligari, Moreno-Insertis, & Schüssler (1995) carried out numerical calculations of flux emergence where the formation of rising flux loops which eventually emerge at the surface as active regions results from the adiabatic growth of an undulatory instability of toroidal flux tubes initially in mechanical equilibrium (neutral buoyancy) in the stable overshoot layer.

The purpose of this paper is to study the effect of radiative heating on the evolution of thin flux tubes and the formation of emerging flux loops. In the convection zone and the overshoot region, convective heat transport results in the mean temperature gradient deviating from that of radiative equilibrium. Hence there will be a non-zero divergence of radiative heat flux, and flux tubes should experience a radiative heating (or cooling) depending on their location; the non-zero divergence of radiative flux causes radiative heating near the bottom of the convection zone, and cooling in the surface layers. Furthermore, the presence of magnetic pressure causes a slight difference of the thermodynamic properties within the flux tube relative to the surrounding field free fluid, as has long been recognized (Parker 1979). For example, a flux tube in the state of neutral buoyancy in the solar interior should have a slightly lower mean temperature within the flux tube than the mean temperature one would otherwise obtain for the same volume of the tube if the flux tube were not there. This slight difference in the thermodynamic properties of the flux tube will cause an additional radiative heating of the tube.

In §2, we evaluate the radiative heating experienced by a thin flux tube in the solar interior and derive a new energy equation for the flux tube. In §3 the effect of the radiative heating on the evolution and storage of toroidal flux tubes in the overshoot layer is studied. In §4 we investigate how emerging flux loops may develop as a result of radiative heating from toroidal flux tubes initially in neutral buoyancy in the overshoot region. Using numer-

ical simulations, we test the following evolutionary scenario. We consider an initial toroidal flux tube with non-uniform thermodynamic properties along the tube and whose depth is also non-uniform in the overshoot region. The presence of such non-uniformities along toroidal flux tubes in the overshoot region seems inevitable since the toroidal tubes probably result from the stretching of initially weaker fields by radial differential rotation. This means that the flux tubes are made up of plasma from slightly different depths and hence slightly different thermodynamic properties. As a result of radiative heating, the toroidal tube should rise quasi-statically, and the top-most portion of the tube will first enter the convection zone while the inner portion of the tube is still in the stable overshoot layer. We find that this process leads to the eruption of an anchored flux loop to the photosphere. Finally in §5, we give a summary and discussion of the main points of the paper.

## 2. Thin Flux Tube Evolution with Radiative Diffusion

The basic equations determining the dynamic evolution of a thin magnetic flux tube in the solar interior have been described in Spruit (1981), Choudhuri (1989), Fan, Fisher, & DeLuca (1993, Paper I), Fan, Fisher, & McClymont (1994, Paper II), and Caligari, Moreno-Insertis, & Schüssler (1995). These papers have all considered adiabatic evolution of the flux tubes. In this paper, we modify the formulation presented in Paper I by incorporating into the energy equation the effects of heating due to radiative diffusion.

The entropy per unit mass of the flux tube plasma is a function of the pressure and density of the plasma, i.e. $S = S(p, \rho)$. Hence the time variation of $S$ can be expressed as:

$$\frac{dS}{dt} = \left(\frac{\partial S}{\partial p}\right)_\rho \frac{dp}{dt} + \left(\frac{\partial S}{\partial \rho}\right)_p \frac{d\rho}{dt}. \tag{1}$$

From the first law of thermodynamics and the Maxwell relations, we obtain:

$$\left(\frac{\partial S}{\partial p}\right)_\rho = \frac{1}{\rho^2}\left(\frac{\partial \rho}{\partial T}\right)_S, \tag{2}$$

$$\left(\frac{\partial S}{\partial \rho}\right)_p = -\frac{1}{\rho^2}\left(\frac{\partial p}{\partial T}\right)_S. \tag{3}$$

Combining equations (1), (2), and (3) yields

$$\frac{1}{\rho}\frac{d\rho}{dt} = \frac{1}{\gamma p}\frac{dp}{dt} - \nabla_{\rm ad}\,\frac{\rho}{p}\,T\frac{dS}{dt}, \tag{4}$$

where $T$ is the temperature of the tube plasma, $\gamma \equiv (\partial \ln p/\partial \ln \rho)_s$, and $\nabla_{\rm ad} \equiv (\partial \ln T/\partial \ln p)_s$. In Paper I we have considered adiabatic evolution with $dS/dt = 0$ and thus the evolution

of the thermodynamic quantities $p$ and $\rho$ of the tube plasma satisfies the simple relation $dp/dt = (\gamma p/\rho)(d\rho/dt)$.

To evaluate the rate of heat input per unit volume of the tube plasma $dQ/dt \equiv \rho T dS/dt$ resulting from radiative diffusion, we consider a locally straight flux tube segment embedded in the background field free plasma. We set up cylindrical polar coordinates ($\varpi$, $\phi$, $s$) with the vertical axis ($s$) being the tube axis, and $\varpi$ and $\phi$ denoting respectively the horizontal radius and azimuthal angle in the tube cross section. The heating rate due to radiative diffusion should be:

$$\frac{dQ}{dt} \;=\; \nabla \cdot (\kappa \nabla T) \;=\; \nabla \cdot (\kappa_e \nabla T_e) + \nabla \cdot (\delta\kappa \nabla T_e) + \nabla \cdot (\kappa \nabla \delta T), \tag{5}$$

where $T_e$ and $\kappa_e$ denote respectively the temperature and radiative conductivity of the unperturbed field free plasma, and $\delta T \equiv T - T_e$ and $\delta\kappa \equiv \kappa - \kappa_e$ represent respectively the changes (or perturbations) in temperature and radiative conductivity introduced within the magnetic flux tube. The expression for the radiative conductivity is

$$\kappa = \frac{16\sigma_s T^3}{3\tilde{\kappa}\rho}, \tag{6}$$

where $\sigma_s$ is the Stefan-Boltzmann constant, and $\tilde{\kappa}$ is the Rosseland mean opacity (in units of $[\mathrm{cm^2 g^{-1}}]$). The first term after the second equality in equation (5) corresponds to radiative heating or cooling by the divergence of radiative flux in the background field free plasma. The second and the third terms reflect the perturbations to the radiative heat flux caused by the presence of the magnetic field in the flux tube. We can rewrite the second and the third terms in the cylindrical coordinates of the flux tube as respectively:

$$\nabla \cdot (\delta\kappa \nabla T_e) = \frac{\partial}{\partial s}\left(\delta\kappa \frac{\partial T_e}{\partial s}\right) + (\nabla_\perp \delta\kappa) \cdot (\nabla_\perp T_e) + \delta\kappa \nabla_\perp^2 T_e, \tag{7}$$

and

$$\nabla \cdot (\kappa \nabla \delta T) = \frac{\partial}{\partial s}\left(\kappa \frac{\partial \delta T}{\partial s}\right) + (\nabla_\perp \kappa_e + \nabla_\perp \delta\kappa) \cdot (\nabla_\perp \delta T) + \kappa \nabla_\perp^2 \delta T, \tag{8}$$

where

$$\nabla_\perp = \left(\frac{\partial}{\partial \varpi},\; \frac{1}{\varpi}\frac{\partial}{\partial \phi},\; 0\right). \tag{9}$$

We now compare the magnitudes of the 6 terms on the right hand sides of equations (7) and (8). We will refer to these terms in order as, respectively, (7)-1, (7)-2, (7)-3, (8)-1, (8)-2, and (8)-3. In the case of thin magnetic flux tubes, the length scale of variation along the tube axis (which is on the order of the pressure scale height $H_p$) is much greater than the radius of the tube cross section $a$. Furthermore, for the thin flux tubes we consider

here, it is generally true that $\delta\kappa/\kappa \sim \delta T/T \ll 1$. For a quantity of the background field free plasma $q_e$ (e.g. $T_e$ and $\kappa_e$), the magnitudes of its derivatives $\partial q_e/\partial s$ and $\nabla_\perp q_e$ (depending on the orientation of the tube) are both estimated to be at most $\sim q_e/H_p$. On the other hand, for each perturbation quantity within the tube $\delta q$ (e.g. $\delta T$ and $\delta\kappa$), we generally have $\partial\delta q/\partial s \sim \delta q/H_p$ and $\nabla_\perp \delta q \sim \delta q/a$. Hence we estimate the magnitudes of terms (7)-1, (7)-2, (7)-3, (8)-1, (8)-2, and (8)-3 as respectively $\sim \delta\kappa\, T_e/H_p^2$, $\delta\kappa\, T_e/(aH_p)$, $\delta\kappa\, T_e/H_p^2$, $\kappa\,\delta T/H_p^2$, $(\kappa_e/H_p + \delta\kappa/a)\,\delta T/a$, and $\kappa\,\delta T/a^2$. Comparing the magnitudes of the 6 terms, we can see that the dominant contribution comes from term (8)-3, $\kappa\nabla_\perp^2\delta T$, and therefore equation (5) can be reduced to

$$\frac{dQ}{dt} \simeq \nabla\cdot(\kappa_e\,\nabla T_e) + \kappa\nabla_\perp^2\delta T. \tag{10}$$

We henceforth denote the two terms on the right hand side of equation (10) as $(dQ/dt)_1$ and $(dQ/dt)_2$ respectively in the following discussion. The term $(dQ/dt)_1$ is determined entirely by the mean temperature distribution in the background plasma and is zero if the fluid is in radiative equilibrium, which is the case in the radiative interior. In the convection zone and the overshoot region, however, the surrounding plasma is not in radiative equilibrium (most of the energy is transported by convection) and the term is generally non-zero. As a result $(dQ/dt)_1$ will cause radiative heating (or cooling) of the flux tube depending on its location. The term $(dQ/dt)_2$ corresponds to radiative diffusion across the flux tube due to the temperature difference between the flux tube and the background field free fluid. Its effect is to reduce the temperature difference.

In the convection zone, $(dQ/dt)_1$ can be evaluated using mixing length formalism (e.g. Mihalas 1978; Spruit 1974):

$$\left(\frac{dQ}{dt}\right)_1 \equiv \nabla\cdot(\kappa_e\,\nabla T_e) = -\nabla\cdot(\mathbf{F}_{\rm rad}) = -\nabla\cdot\left(\frac{\bigtriangledown}{\bigtriangledown_{\rm rad}}\mathbf{F}_{\rm tot}\right) = -F_{\rm tot}\frac{d}{dr}\left(\frac{\bigtriangledown}{\bigtriangledown_{\rm rad}}\right) \tag{11}$$

where $\mathbf{F}_{\rm rad}$, $\mathbf{F}_{\rm tot}$, $\bigtriangledown_{\rm rad} \equiv (d\ln T_e/d\ln p_e)_{\rm rad}$, and $\bigtriangledown \equiv d\ln T_e/d\ln p_e$ denote respectively the radiative energy flux, the total energy flux, the radiative equilibrium temperature gradient, and the actual temperature gradient in the background convection zone. Here, $p_e$ is the pressure in the external field free plasma, $r$ denotes the radial distance from the center of the sun, and the magnitude of $\mathbf{F}_{\rm tot}$ is $F_{\rm tot} = L/(4\pi r^2)$, with $L$ being the total luminosity of the sun. For the last equality in equation (11), the requirement $\nabla\cdot(\mathbf{F}_{\rm tot}) = 0$ has been used. In Figure 1 we plot the result of equation (11) as a function of the height above the base of the convection zone. The result is computed from the variations of $\bigtriangledown$ and $\bigtriangledown_{\rm rad}$ as functions of $r$ in Spruit's mixing length model of the solar convection zone (Spruit 1974). It can be seen that $(dQ/dt)_1$ heats the flux tube in the lower part of the convection zone, and cools the flux tube in the surface layer.

To evaluate $(dQ/dt)_1$ in the overshoot region, we can still use equation (11). The exact temperature stratification in the overshoot region is very uncertain, but we know that the essential effect of convective overshooting is to maintain $\bigtriangledown$ in the overshoot layer (whose thickness is $\sim$ a few tenths of $H_p$) very close to its adiabatic value $\bigtriangledown_{\rm ad}$ (see e.g. van Ballegooijen 1982, Schmitt, Rosner, & Bohn 1984). In other words, $\delta \equiv \bigtriangledown - \bigtriangledown_{\rm ad}$ is negative, but its absolute value is maintained very close to zero (probably not exceeding $10^{-4}$) across the depth of the overshoot region beneath the convection zone base (where $\delta = 0$); only when reaching the boundary between the overshoot region and the radiative interior does the magnitude of $\delta$ jump sharply to the radiative value. It is therefore reasonable to assume that within the overshoot region, $|d\delta/dr| < 10^{-4}/H_p$. From equation (11) we have in the overshoot region:

$$\left(\frac{dQ}{dt}\right)_1 = -F_{\rm tot}\left(\frac{1}{\bigtriangledown_{\rm rad}}\frac{d\delta}{dr} - \frac{\bigtriangledown}{\bigtriangledown_{\rm rad}^2}\frac{d\bigtriangledown_{\rm rad}}{dr}\right), \tag{12}$$

in which we have used the fact that $\bigtriangledown_{\rm ad}$ is almost constant across the overshoot region. The magnitude of the first term inside the right hand side brackets of equation (12) is $\lesssim 10^{-4}/(\bigtriangledown_{\rm rad}H_p)$, and the magnitude of the second term is $\sim \bigtriangledown/(\bigtriangledown_{\rm rad}H_p)$. Since $\bigtriangledown \sim 0.4 \gg 10^{-4}$, we neglect the first term and obtain

$$\left(\frac{dQ}{dt}\right)_1 \simeq F_{\rm tot}\frac{\bigtriangledown}{\bigtriangledown_{\rm rad}^2}\frac{d\bigtriangledown_{\rm rad}}{dr}. \tag{13}$$

The above quantity does not change significantly across the thin overshoot region. Hence, we can evaluate it at the base of the convection zone and use the resulting value as the heating rate $(dQ/dt)_1$ in the overshoot region. From

$$F_{\rm tot} = \kappa_e\frac{T_e}{H_p}\bigtriangledown_{\rm rad} \tag{14}$$

we have

$$\bigtriangledown_{\rm rad} = F_{\rm tot}\frac{R}{\mu g}\frac{1}{\kappa_e}, \tag{15}$$

where, $R$, $\mu$, and $g$ are respectively the gas constant, the mean molecular weight, and the local gravitational acceleration. Because $g$ and $F_{tot}$ both scale roughly as $r^{-2}$, the coefficient in front of $1/\kappa_e$ in equation (15) is essentially constant. Then

$$\frac{d\bigtriangledown_{\rm rad}}{dr} = -F_{\rm tot}\frac{R}{\mu g}\frac{1}{\kappa_e}\frac{d\ln\kappa_e}{dr}. \tag{16}$$

To evaluate $d\ln\kappa_e/dr$ at the base of the convection zone, we consider Krammer's opacity law (see e.g. Schwarzschild 1957): $\tilde{\kappa}_e \propto \rho_e^n T_e^{-m}$ with $n = 1$ and $m = 3.5$, and from equation (6) we obtain $\kappa_e \propto T_e^{6.5}\rho_e^{-2}$. Therefore,

$$\frac{d\ln\kappa_e}{dr} = 6.5\,\frac{d\ln T_e}{dr} - 2\,\frac{d\ln\rho_e}{dr} = -\left(6.5\bigtriangledown_{\rm ad} - \frac{2}{\gamma}\right)\frac{1}{H_p}. \tag{17}$$

Combining equations (13), (16), and (17) and applying the appropriate values at the base of the convection zone, we find

$$\left(\frac{dQ}{dt}\right)_1 \simeq 29.7 \text{ erg cm}^{-3} \text{ s}^{-1} \tag{18}$$

for the overshoot region. This value is nearly equal to the heating rate just above the base of the convection zone (Figure 1) because $\bigtriangledown$ is close to the adiabatic value $\bigtriangledown_{\rm ad}$ within models of the overshoot region.

To compute the heating rate $(dQ/dt)_2 \equiv \kappa \nabla_\perp^2 \delta T$ in the context of the thin flux tube approximation, we need to express it in terms of the mean difference $\overline{\delta T}$ between the internal and background mean temperatures $\overline{T}$ and $\overline{T}_e$ averaged over the tube cross section. For this purpose, we assume that the profile of $\delta T$ over the tube cross section follows $AJ_0(k_1\varpi)$, where $A$ is a constant, $k_1$ satisfies $k_1 a = x_1$, with $x_1$ being the first zero of Bessel function $J_0(x)$. This profile corresponds to the slowest decaying mode in the solutions of the linear thermal diffusion equation across a cylindrical tube embedded in a fixed external temperature. Taking the average of $\kappa \nabla_\perp^2 \delta T$ over the tube cross section and in doing so approximating $\kappa$ as a constant whose value equals to $\kappa_e$ at the position of the tube axis, we obtain

$$\left(\frac{dQ}{dt}\right)_2 = -\kappa_e \frac{x_1^2}{a^2} (\overline{T} - \overline{T}_e), \tag{19}$$

where for $\overline{T}_e$ we simply take the local value of $T_e$ at the position of the tube axis.

We can compare the magnitudes of the two major heating terms $(dQ/dt)_1$ and $(dQ/dt)_2$ to examine their relative importance. The term $(dQ/dt)_1$ is only a function of position in the background fluid and its magnitude is

$$\left| -F_{\rm tot} \frac{d}{dr} \left( \frac{\bigtriangledown}{\bigtriangledown_{\rm rad}} \right) \right| \sim \left( \kappa_e \frac{T_e}{H_p} \bigtriangledown_{\rm rad} \right) \left( \frac{\bigtriangledown}{\bigtriangledown_{\rm rad}} \frac{1}{H_p} \right) \sim \kappa_e \bigtriangledown \frac{T_e}{H_p^2}. \tag{20}$$

On the other hand the magnitude of $(dQ/dt)_2$ is $\sim \kappa \, \delta T / a^2$, which varies with the cross sectional radius of the flux tube. The ratio of $|(dQ/dt)_1|$ over $|(dQ/dt)_2|$ is therefore $\sim \bigtriangledown (\delta T/T_e)^{-1} (a/H_p)^2$, where $\bigtriangledown \sim 0.4$. For a neutrally buoyant flux tube in the lower convection zone or overshoot region, $(\delta T/T_e)^{-1} \sim \beta \equiv p_e/(B^2/8\pi)$ where $B$ is the field strength of the flux tube. With typical values of $B$ ranging from $10^4$ to $10^5$ G, and total flux $\Phi$ from $10^{20}$ to $10^{22}$ Mx, $\beta$ varies from about $1.5 \times 10^7$ to $1.5 \times 10^5$ and $(a/H_p)^2 = \Phi/\pi B H_p^2$ varies from 0.01 to $10^{-5}$. Therefore we typically have $|(dQ/dt)_1 \ / \ (dQ/dt)_2| \sim \beta (a/H_p)^2 \gg 1$, meaning that $(dQ/dt)_1$ is generally larger in magnitude than $(dQ/dt)_2$. This more important heating term $(dQ/dt)_1$ has hitherto been neglected in earlier studies of the storage and rising of flux tubes in the solar interior, where typically only the effect of

$(dQ/dt)_2$ was considered. The large magnitude of $(dQ/dt)_1$ in the overshoot region and right above the bottom of the convection zone (see Figure 1) will have a significant consequence for the storage of toroidal flux tubes in the overshoot region and on the development of erupting magnetic flux loops in the deep convection zone. Note that although $(dQ/dt)_2$ depends sensitively on the radius $a$ of the tube cross section as can be seen from equation (19), the much larger $(dQ/dt)_1$ resulting from the non-radiative-equilibrium external temperature gradient is a function only of position (see eq. [11] and Figure 1) and does not depend on the width of the tube. Hence the total radiative heating of tube plasma becomes insensitive to the width of the tube.

Combining equations (4), (10), and (19), we obtain the energy equation for the thin flux tube model:

$$\frac{1}{\rho}\frac{d\rho}{dt} = \frac{1}{\gamma p}\frac{dp}{dt} - \nabla_{\rm ad}\frac{1}{p}\left[\left(\frac{dQ}{dt}\right)_1 - \kappa_e \frac{x_1^2}{a^2}(T - T_e)\right]. \tag{21}$$

Here we have omitted the overbar denoting average temperatures, noting that all physical quantities (e.g. $p$, $\rho$, and $T$) inside the flux tube represent an average over the tube cross section as is assumed in the thin flux tube approximation. In the above, $(dQ/dt)_1$ is computed from equation (11) using Spruit's mixing length model in the convection zone, and takes the constant rate of 29.7 erg cm$^{-3}$ s$^{-1}$ in the overshoot region, $x_1 \simeq 2.40$, $a^2 = \Phi/(\pi B)$ where $\Phi$ and $B$ are respectively the total flux and field strength of the flux tube, and $\kappa_e$ is given by equation (6) in which $\tilde{\kappa}$, $T$, and $\rho$ are approximated by their local external values at the location of the tube axis.

Regarding the equation of motion for the thin flux tube, there has been much discussion of how to best treat the apparent added inertia of the flux tube caused by its motion relative to the surrounding fluid (cf. Cheng 1992; Ferris-Mas & Schüssler 1994; Paper II; Caligari, Moreno-Insertis, & Schüssler 1995). In Paper II we derived an equation of motion which corrected the defects in the earlier treatments of the added inertia to avoid spurious terms resulting from the longitudinal motion of the tube plasma (which should not disturb the external fluid). Recently Caligari, Moreno-Insertis, & Schüssler (1995) have taken the approach of simply neglecting the added inertia effect, arguing that it is unimportant because it plays a significant role only in the rapidly accelerating phases of motion which occur rarely during the evolution of the tube. By carrying out a series of flux tube simulations using both the equation of motion derived in Paper II and the equation with the added inertia neglected, we find that the results are not substantially different, with the quantitative difference (in e.g. rise time, latitude of emergence, and tilt angle) amounting to a few percent. Hence for this paper, we have taken the same approach as Caligari, Moreno-Insertis, & Schssler (1995) and have ignored added inertia effects in the equation of motion.

The equations we use to determine the evolution of the thin flux tube are the following:

$$\rho\frac{d\mathbf{v}}{dt} = -2\rho(\mathbf{\Omega}\times\mathbf{v}) - (\rho_e-\rho)[\mathbf{g}-\mathbf{\Omega}\times(\mathbf{\Omega}\times\mathbf{r})] + \mathbf{l}\frac{\partial}{\partial s}\left(\frac{B^2}{8\pi}\right) + \frac{B^2}{4\pi}\mathbf{k} - C_d\frac{\rho_e|\mathbf{v}_\perp|\mathbf{v}_\perp}{\pi(\Phi/B)^{1/2}}, \quad (22)$$

$$\frac{d}{dt}\left(\frac{B}{\rho}\right) = \frac{B}{\rho}\left[\frac{\partial(\mathbf{v}\cdot\mathbf{l})}{\partial s} - \mathbf{v}\cdot\mathbf{k}\right], \quad (23)$$

$$\frac{1}{\rho}\frac{d\rho}{dt} = \frac{1}{\gamma p}\frac{dp}{dt} - \bigtriangledown_{\rm ad}\frac{1}{p}\left[\left(\frac{dQ}{dt}\right)_1 - \kappa_e\, x_1^2\,\pi\,\frac{B}{\Phi}\,(T-T_e)\right], \quad (24)$$

$$p = \frac{\rho RT}{\mu}, \quad (25)$$

$$p + \frac{B^2}{8\pi} = p_e, \quad (26)$$

where $\mathbf{r}$, $\mathbf{v}$, $B$, $p$, $\rho$, $T$ denote respectively the position, velocity, field strength, pressure, density and temperature of the tube plasma, each of which is a function of time $t$ and the arc-length $s$ measured along the tube, $\mathbf{l}\equiv\partial\mathbf{r}/\partial s$ is the unit vector tangential to the flux tube and $\mathbf{k}\equiv\partial^2\mathbf{r}/\partial s^2$ is the tube's curvature vector, $\mathbf{v}_\perp$ is the component of $\mathbf{v}$ perpendicular to the flux tube, $\Phi$ is the constant total flux of the tube, $p_e$, $\rho_e$, and $T_e$ are respectively the pressure, density and temperature of the local surrounding field free plasma, $\mathbf{g}$ is the gravitational acceleration, $\mathbf{\Omega}$ is the angular velocity of the reference frame corotating with the sun, and $C_d$ is the drag coefficient, which is set to unity. In comparison with Paper I, the differences in the basic equations are 1) the new energy equation (eq. [24]) which takes into account heat transport by radiative diffusion, and 2) the neglect of added inertia in the equation of motion (eq. [22]). The equation of motion here is consistent with that of Ferris-Mas & Schüssler (1994) and Caligari, Moreno-Insertis, & Schüssler (1995), except that we only consider the solid body rotation of the sun (which corotates with our frame of reference) and neglect the external flow field resulting from differential rotation. The remaining equations (eqs. [23], [25], [26]), which result respectively from mass conservation and the induction equation, the ideal gas law, and the requirement of instantaneous pressure balance, are the same as those in Paper I.

The numerical method used to solve for the flux tube evolution as determined by the above set of equations has been described in detail in Paper I. The physical conditions for the external field free plasma, namely $g$, $p_e$, $\rho_e$, $T_e$, temperature gradient $\bigtriangledown\equiv d\ln T_e/d\ln p_e$ and its corresponding adiabatic value $\bigtriangledown_{\rm ad}$, and $\delta\equiv\bigtriangledown-\bigtriangledown_{\rm ad}$, at any given depth in the convection zone are obtained from Spruit's model of the solar convection zone (Spruit 1974). We approximate the thin overshoot region below the base of the convection zone by a subadiabatically stratified polytrope with a constant $\delta=-3.6\times10^{-5}$, and constant $g$ and $\bigtriangledown_{\rm ad}$ which are equal to their values at the base of the convection zone. The precise

amplitude and variation of $\delta$ in the overshoot region is very uncertain. The value we use here is within the possible range of $\delta$ suggested by various theoretical models of the overshoot region (e.g. Shaviv & Salpeter 1973; van Ballegooijen 1982).

## 3. Upward Drift of Toroidal Flux Tubes in the Overshoot Region

Before carrying out numerical calculations of the eruption of magnetic flux loops to the surface, we first consider the upward drift of a toroidal flux tube in the overshoot region as a result of heating by radiative diffusion. As discussed in the previous section, convective overshooting modifies the mean temperature stratification in the overshoot region to closely follow the adiabatic gradient. Hence the background temperature gradient deviates from that of the radiative equilibrium and the convergence of the radiative flux results in a heating of the flux tube. We have found in the previous section that this is the dominant source of heating experienced by the flux tube, and its rate is estimated to be $(dQ/dt)_1 = 29.7$ erg cm$^{-3}$ s$^{-1}$ in the overshoot region. If the flux tube is originally in neutral buoyancy ($\rho = \rho_e$), the heating will increase the specific entropy within the flux tube, resulting in a decrease in the density, and hence a rising motion of the tube.

From equations (23), (24), and (26) we can derive the following general expression for the density difference $\Delta\rho \equiv \rho_e - \rho$ between the flux tube and the background plasma:

$$\begin{aligned}\frac{d\Delta\rho}{dt} =& \rho_e \frac{v_r}{H_p}\left[\delta + \left(\frac{1}{\gamma} - \frac{2}{\gamma^2}\right)\frac{1}{\beta} - \frac{1}{\gamma}\frac{\Delta\rho}{\rho_e}\right] + \frac{2}{\gamma\beta}\rho_e\left[\frac{\partial(\mathbf{v}\cdot\mathbf{l})}{\partial s} - \mathbf{v}\cdot\mathbf{k}\right] \\ &+ \frac{\rho_e}{p_e}\bigtriangledown_{\rm ad}\left[\left(\frac{dQ}{dt}\right)_1 - \kappa_e x_1^2 \pi \frac{B}{\Phi}(T - T_e)\right],\end{aligned} \tag{27}$$

where $v_r$ is the radial velocity of the flux tube. In deriving the above equation, we have used $dp_e/dr = -\rho_e g$ and we have only retained terms to first order in the quantities $\Delta\rho/\rho_e$ and $1/\beta \equiv B^2/8\pi p_e$, since their magnitudes are much less than 1. We can ignore the second heating term in the last square brackets of equation (27) since it is generally much smaller in magnitude than the first term. Due to the subadiabatic stratification $\delta < 0$ in the overshoot region, the first term on the right hand side of equation (27) will cause the buoyancy of the flux tube ($\Delta\rho$) to decrease as the tube rises. If the heating rate is not too fast, i.e. if the time scale for the heating to significantly change the temperature difference between the flux tube and the back ground fluid (the thermal time scale) is long compared to the dynamic time scale characterized by the magnetic Brunt-Väisälä frequency $\omega_B$ (Ferris-Mas & Schüssler 1994) where

$$\omega_B^2 = -\frac{g\delta}{H_p} + \frac{v_a^2}{H_p^2}\left[\frac{2}{\gamma}\left(\frac{1}{\gamma} - \frac{1}{2}\right)\right], \tag{28}$$

with $v_a^2 = B^2/4\pi\rho_e$, then the rise of the flux tube can be considered as quasi-static, i.e. the tube evolves through a series of mechanical equilibrium states with $\Delta\rho$ remaining very close to zero as the tube rises. The thermal time scale can be estimated as

$$\tau_{\rm th} \sim |\delta T| \left[\frac{1}{c_p\rho_e}\left(\frac{dQ}{dt}\right)_1\right]^{-1} \sim \frac{1}{\beta}T_e\left[\frac{1}{c_p\rho_e}\left(\frac{dQ}{dt}\right)_1\right]^{-1}, \tag{29}$$

where $c_p$ is the heat capacity per unit mass at constant pressure. The dynamic time scale on the other hand, is $\tau_B \equiv 2\pi/\omega_B$. If we consider flux tubes with $B = 60$ kG, and subadiabaticity $\delta = -3.6 \times 10^{-5}$, then $\tau_{th} \sim 10^7$ s and $\tau_B \sim 4 \times 10^5$ s. Since $\tau_{\rm th}$ is significantly larger than $\tau_B$, a quasi-static rise is a good assumption for the evolution of these tubes.

In the case of quasi-static rising, we can set $(d/dt)(\Delta\rho)$ and $\Delta\rho$ to zero in equation (27). Furthermore, for simplicity, we consider the rise of a uniform horizontal flux tube in a plane parallel overshoot region. Thus we have $\partial(\mathbf{v}\cdot\mathbf{l})/\partial s = 0$ and $\mathbf{v}\cdot\mathbf{k} = 0$ in equation (27). We then obtain

$$v_r = H_p \bigtriangledown_{\rm ad} \frac{1}{p_e}\left(\frac{dQ}{dt}\right)_1 \left[|\delta| + \left(\frac{2}{\gamma^2} - \frac{1}{\gamma}\right)\frac{1}{\beta}\right]^{-1}. \tag{30}$$

We can see that $v_r$ does not vary sensitively with the field strength if the term $(2/\gamma^2 - 1/\gamma)(1/\beta) \approx 0.12(1/\beta)$ is small compared to $|\delta|$, which is the case as long as $B \lesssim 10^5$G and $|\delta| \gtrsim 10^{-6}$. Applying the appropriate values at the base of the convection zone to equation (30), we obtain $v_r \approx 1.2 \times 10^{-3}|\delta|^{-1}$ which gives $\sim 30$ cm s$^{-1}$ if $\delta = 3.6 \times 10^{-5}$. With this rise speed, flux tubes will escape from the overshoot region (assuming the depth is $\sim 10^9$ cm) in a time scale of $\sim 1$ year. This time scale will be further shortened if the absolute value of $\delta$ in the overshoot region is smaller. The rather short storage time ($\sim 1$ year) for toroidal flux tubes in the overshoot region is caused by the large radiative heating rate resulting from the non-radiative-equilibrium temperature gradient in the layer. If this scenario is indeed true, then it has significant implications for the nature of the solar dynamo. One possibility for increasing the storage time is that the magnitude of $\delta$ is significantly larger. For example, an order of magnitude increase in the absolute value of $\delta$ to $\delta = -3.6 \times 10^{-4}$ in the overshoot region would increase the storage time to $\sim 10$ year, which becomes comparable to the length of the solar cycle. It is likely that the presence of strong magnetic flux tubes in the overshoot region can suppress the convective motions significantly so that $|\delta|$ is increased. In the vicinity of the flux tube, the temperature gradient may be so substantially altered that it approaches radiative equilibrium and hence the radiative heating itself is greatly reduced. However, the time scale for the temperature gradient around the flux tube to be altered substantially in response to the presence of a tube which

can suppress convection, should be similar to the time scale for the radiative heating of the flux tube itself. Therefore we believe that the radiative heating $(dQ/dt)_1$ due to the non-radiative-equilibrium temperature gradient in the overshoot region is playing an important role in causing the upward drift and escape of strong toroidal flux tubes, although $(dQ/dt)_1$ may not simply consist of a constant, uniform heating rate. Clearly, further investigation on the influence of strong toroidal flux tubes on convective overshooting and the temperature stratification in the overshoot region is needed.

Having estimated the mean upward drift velocity of a toroidal flux tube in the overshoot region by considering the quasi-static rise of a uniform horizontal flux tube, we now turn to numerical simulations to study the evolution of a non-uniform toroidal flux tube lying in the overshoot region. We will investigate the eruption of "Ω" shaped flux loops from the toroidal tubes as a result of radiative heating.

## 4. Numerical Simulations of Loop Eruption

4.1 *Initial conditions and the non-linear development of emerging loops*

The initial position of the toroidal flux ring in the overshoot region is described by

$$r = r_0 + \Delta r_0 \, exp \left\{ - \left[ \frac{2(\phi - \phi_0)}{\Delta \phi} \right]^2 \right\}, \tag{31}$$

$$\theta = \theta_0 , \tag{32}$$

where $r$ denotes the radial distance from the center of the sun, $\theta$ denotes latitude, $\phi$ denotes longitude. The majority (hereafter the "uniform portion") of the ring is located at a depth corresponding to radial distance $r_0$, while a smaller part (hereafter the "non-uniform portion") of the ring with length scale $\lambda \equiv r_0 \Delta\phi$ protrudes into shallower depths, with $\Delta r_0$ denoting the maximum depth difference. In this study, we let $r_0$ be at $5 \times 10^8$ cm below the base of the convection zone, and we let $\lambda = 5 \times 10^{10}$ cm and $\Delta r_0 = 5 \times 10^8$ cm so the apex of the ring is at the base of the convection zone. For the thermodynamic properties of the initial toroidal ring, we assume that the density of the tube plasma is equal to its local external density $\rho = \rho_e$, i.e the buoyancy force is initially zero everywhere. Along the field lines, the tube plasma is assumed to be initially in hydrostatic equilibrium, i.e. $\partial p/\partial s = \rho \, (\mathbf{g} \cdot \mathbf{l})$, which leads to $\partial \, (B^2/8\pi)/\partial s = (\rho_e - \rho) \, (\mathbf{g} \cdot \mathbf{l})$ because of the requirements of pressure balance (eq. [26]) and hydrostatic equilibrium of the external plasma $\partial p_e/\partial s = \rho_e \, (\mathbf{g} \cdot \mathbf{l})$. Since $\rho = \rho_e$ initially, the magnetic field strength $B_0$ should be constant along the flux tube. We let the uniform portion of the initial ring be in mechanical equilibrium, with the buoyancy force equal to zero and the tension force balanced by the Coriolis force and centrifugal force. Thus we assume that the initial ring is rotating as a

whole at a constant angular velocity $\omega_0$ in the direction of solar rotation relative to the external plasma, i.e. the ring has a longitudinal motion with

$$v_\phi = \omega_0 \, r \, \cos\theta_0 . \tag{33}$$

The magnitude of the angular velocity $\omega_0$ is specified such that for the uniform portion of the ring located at radius $r_0$ the centrifugal and Coriolis forces of the tube plasma resulting from $v_\phi$ are balancing the tension force, i.e.

$$\omega_0^2 \, r_0^2 \, \cos^2\theta_0 + 2\omega_0 \Omega \, r_0^2 \, \cos^2\theta_0 - \frac{B_0^2}{4\pi\rho} = 0. \tag{34}$$

For the non-uniform portion of the ring, the buoyancy force is also zero, but the tension, centrifugal and Coriolis forces generally do not balance exactly, and the shape of the ring will re-adjust in the subsequent evolution which we will compute numerically.

Figure 2 shows the subsequent motion of a toroidal flux ring with initial conditions described above. The toroidal ring has an initial field strength $B_0 = 60$ kG, total flux $\Phi = 10^{22}$ Mx, initial latitude $\theta_0 = 5°$, and its apex is initially located at longitude $\phi_0 = 180°$. From equation (34) the initial angular velocity of the toroidal ring is $\omega_0 = 1.037 \times 10^{-7}$ rad $s^{-1}$. In Figure 2(a) the successive positions of the toroidal ring in the $r$-$\phi$ plane are shown at time instances $t = 0$, 23, 45, 68, and 83 days. We find that an emerging flux loop is formed from the initial toroidal ring and reaches the photosphere after a total elapsed time of 83 days. In comparison, Figure 2(b) shows the motion of the toroidal ring if the effect of radiative heating is ignored and adiabatic evolution is assumed. The successive positions of the ring at uniformly spaced times (with an interval of 2 months) are shown in Figure 2(b). The re-adjustment of the shape of the ring due to the initial imbalance of forces in the non-uniform portion of the ring is quite complicated and small oscillations are present in the subsequent evolution. However, it can be seen in Figure 2(b) that overall the change in the shape of the ring is small and the ring as a whole precesses in the direction of rotation at roughly the initial rate $\omega_0$. We can understand this relatively small change in the shape of the ring as follows: At the ring apex, the tension force is initially slightly greater than the sum of the centrifugal and Coriolis forces and as a result the apex subsequently reduces its height, gaining sufficient buoyancy to counteract the excess in the tension force. One can estimate the necessary decrease in height, which gives a measure of the subsequent change in the shape of the ring. The initial excess in the tension force at the apex compared to the uniform part of the toroidal ring is of order $(B_0^2/4\pi)(8\Delta r_0/\lambda^2)$. Given the subadiabatic stratification of $\delta = -3.6 \times 10^{-5}$ in the overshoot region, the increase in buoyancy of a mass element as a result of a small decrease in height of $\Delta r$ is $\sim \rho_e g \delta (\Delta r / H_p)$, where $H_p$

is the local pressure scale height. Equating the above excess in tension and the increase in buoyancy, we obtain $\Delta r/\Delta r_0 \sim (16/\beta\delta)(H_p/\lambda)^2$, where $1/\beta \equiv B_0^2/8\pi p_e$. With the specification of the initial parameters stated above, the ratio $\Delta r/\Delta r_0 \sim 10^{-2} \ll 1$, i.e. the change in the shape of the ring is very small. In the case of adiabatic evolution, the toroidal ring therefore essentially maintains its initial configuration, and precesses in the direction of rotation roughly at the constant rate $\omega_0$ as shown in Figure 2(b).

With radiative heating accounted for (Figure 2[a]), the ring, in addition to precessing in the direction of rotation, also rises quasi-statically due to heating and expansion (as suggested in the previous section). The apex of the loop structure first enters the convection zone, while the inner uniform portion of the ring remains within the subadiabatic overshoot region. As a result of entering the convection zone, the upper portion of the loop structure experiences an additional growth of buoyancy resulting from the local superadiabaticity $\delta > 0$, hence the height of the loop apex relative to the inner portion of the ring begins to increase, and a rising flux loop develops. Figure 3(a) shows the radial position of the apex of the loop as a function of time. Figure 3(b) shows the radial accelerations at the loop apex resulting from buoyancy $[(\rho_e - \rho)/\rho]g$ (solid curve), magnetic tension $(B^2/4\pi\rho)(\mathbf{k}\cdot\hat{\mathbf{r}})$ (dashed curve), and the sum of Coriolis and centrifugal forces $-2(\mathbf{\Omega}\times\mathbf{v})\cdot\hat{\mathbf{r}} + v_\phi^2/r$ (dash-dotted curve) as a function of time. The total radial acceleration from the sum of all the forces is also shown (as '+'s). We find that during the earlier stage of the evolution (roughly the first 2 months where $r_{\rm apex} < 0.79R_\odot$), the motion of the apex of the loop is essentially quasi-static with all the forces closely balanced. The growth of buoyancy balances the growth of tension as the height of the loop increases. The superadiabaticity $\delta$ $(> 0)$ in the convection zone increases with height. When the loop apex rises quasi-statically to the height where $\delta$ is sufficiently large, then the growth of buoyancy with height becomes greater than that of the tension force. Unstable eruption of the flux loop then takes place. During this latter dynamic stage of the evolution, the rising speed of the loop is mainly determined by a balance of buoyancy with the aerodynamic drag, and it takes roughly 23 days for the loop apex to traverse from about $0.79R_\odot$ to the surface (see Figure 3).

To see the relative importance of the effect of radiative heating in the rise of the flux loop, we have shown in Figure 4 a comparison between the rate of buoyancy growth $d\Delta\rho/dt$ at the loop apex resulting from radiative heating and that resulting from the adiabatic expansion of the tube plasma, as a function of the position of loop apex in the convection zone. From equation (27), we find that the growth of buoyancy $(d\Delta\rho/dt)_{\rm rad}$ (solid line) due to radiative heating is given by

$$\left(\frac{d\Delta\rho}{dt}\right)_{\rm rad} = \frac{\rho_e}{p_e}\nabla_{\rm ad}\left[\left(\frac{dQ}{dt}\right)_1 - \kappa_e x_1^2 \pi \frac{B}{\Phi}(T - T_e)\right]. \qquad (35)$$

On the other hand, the growth of buoyancy $(d\Delta\rho/dt)_{\rm ad}$ (dashed line) caused by the adiabatic expansion of plasma rising in a superadiabatically stratified surrounding is represented by the first term on the right hand side of equation (27):

$$\left(\frac{d\Delta\rho}{dt}\right)_{\rm ad} = \rho_e \frac{v_r}{H_p}\delta. \tag{36}$$

A comparison of the above two quantities gives an estimate of the relative importance of radiative heating as compared to the adiabatic effects during the evolution of the flux loop. In the right hand side square bracket of equation (35), $(dQ/dt)_1$ dominates the second term corresponding to $(dQ/dt)_2$ throughout the rise of the tube and hence the result of $(d\Delta\rho/dt)_{\rm rad}$ shown in Figure 4 is essentially determined entirely by $(dQ/dt)_1$, which as shown earlier is only a function of position (see Figure 1) and does not depend on the width of the flux tube. We can see from Figure 4 that during the quasi-static stage ($r_{\rm apex} \lesssim 0.79 R_\odot$) of the evolution, $(d\Delta\rho/dt)_{\rm rad}$ is significantly greater than $(d\Delta\rho/dt)_{\rm ad}$, indicating that the growth of buoyancy due to radiative heating is essential in counteracting the magnetic tension and in the rise of the flux loop. As the rise of the loop enters the dynamic stage ($r_{\rm apex} \gtrsim 0.79 R_\odot$), $(d\Delta\rho/dt)_{\rm ad}$ becomes much greater than $(d\Delta\rho/dt)_{\rm rad}$, i.e. radiative heating ceases to be important and the rise of the flux loop can be accurately described by adiabatic evolution. This change to essentially adiabatic evolution is caused by the substantial increases in the superadiabaticity $\delta$ and tube rise speed $v_r$, and also by the decrease in the heating rate $(dQ/dt)_1$.

Figure 5 shows the total rise time, i.e. the time elapsed since the initial state of the toroidal ring until emergence of the loop apex to the surface, as a function of the initial field strength $B_0$, for different values of initial latitudes ($\theta_0 = 1^\circ$ ,$15^\circ$, and $30^\circ$) and total flux ($\Phi = 10^{21}$ and $10^{22}$ Mx). We can see that the variation of the rise time is not large, ranging between 2 to 4 months. The rise times obtained here should not be directly compared with those obtained in Paper I and II where the initial flux tubes were already rendered buoyant by assuming initial thermal equilibrium and the rise times were essentially determined by the balance between buoyancy and drag. There the rise time decreases with field strength $B_0$ because the buoyancy is $\sim B_0^2/8\pi H_p$, and it decreases with flux $\Phi$ because the drag force $\propto \Phi^{-1/2}$. In the present scenario of loop eruption, the unstable loop develops gradually from the initial toroidal flux tube in neutral buoyancy in the overshoot region as a result of radiative heating. As discussed earlier, the rise of the flux loop goes through two distinctive stages of the evolution during which different sets of forces dominate. A large part of the rise time is spent in the quasi-static stage of the evolution during which the growth of buoyancy caused by the radiative heating is playing an important role in counteracting the growth of tension as the loop rises. Only when the superadiabaticity $\delta$ becomes sufficiently

large that the growth of buoyancy dominates the growth of tension and the rise of the loop enters the dynamic stage does the evolution become essentially adiabatic. During this stage, the balance between buoyancy and drag determines the rise speed of the loop. The dependence of the rise time on $B_0$ and $\Phi$ hence become more complicated because of the interplay of various counteracting forces which have different dependences on $B_0$ and $\Phi$. However we find that the overall range of variation of the rise time is significantly smaller because the dominant heating rate $(dQ/dt)_1$ during the earlier quasi-static development of the flux loop is a function of depth only, and does not vary with field strength or flux of the tube. Due to the non-linear nature of the development of the emerging flux loop, we resort to numerical simulations to gain some physical insights into the process. The fairly short rise time (2-4 months) obtained from our set of simulations using reasonable values of the initial parameters suggests that radiative heating is an effective way of causing the eruption of magnetic flux loops to the surface.

4.2 *Properties of the emerging loops*

In this section we present the main properties of the final emerging flux loops developed through the process discussed above. These properties are in general similar to those found from previous investigations using different types of initial conditions, and assuming adiabatic evolution.

Figure 6 shows the emerging latitude of the loops as a function of the initial latitude, with initial field strengths $B_0 = 30$, 60, and 100 kG, and flux $\Phi = 10^{21}$ and $10^{22}$ Mx. As also found in Paper II, the latitudes of loop emergence are consistent with the observed active region latitudes.

The tilt angle of the emerging loops computed from our simulations are shown in Figure 7 as a function of the emerging latitude. The two panels show respectively the cases with $\Phi = 10^{22}$ Mx and $\Phi = 10^{21}$ Mx. The numbers used as data point symbols in the plot indicate the values of initial field strength $B_0$ in units of 10 kG ('X' corresponds to $B_0 = 100$ kG). Here, positive tilt angles correspond to leading side of the loop being equatorward relative to the following side. We find that flux loops with initial field strength $B_0 \gtrsim 40$ kG show tilt angles consistent with the observed mean tilt angles of active regions as described by the Joy's law (see e.g. Howard, 1991). The positive tilt angles are greater for loops with larger flux values, consistent with the finding in Paper II. For weaker initial field strength (e.g. $B_0 = 30$ kG), the emerging loops show negative tilt angles. As discussed in Paper II, the negative tilt angles are caused by the Coriolis force acting upon a converging parallel flow (or upflow) of tube plasma near the loop apex which sets in when the loop becomes hotter than the external plasma (see Appendix B of Paper II). The converging flow sets in earlier and is stronger for loops with weaker initial field strengths, and in Paper II we found

that it causes negative tilts when $B_0 < 20$ kG. Here, because of the additional radiative heating experienced by the flux loop, the converging flow is enhanced and causes loops with initial field $B_0 \lesssim 40$ kG to show negative tilt angles. For larger values of $B_0$, the tilt angle saturates, and tilt angles are essentially equal for $B_0$ between 60 and 100 kG. This result differs significantly from Paper II, assuming initial thermal equilibrium, where we found the tilt angle scaled roughly as $B_0^{-5/4}$.

Figure 8 presents three examples of the final configuration of the emerging loop as viewed from the north pole of the sun. Panels (a), (b), and (c) correspond respectively to the cases with $B_0 = 30$, 60, and 100 kG. For all three cases shown here, the flux $\Phi = 10^{22}$ Mx, the initial latitude $\theta_0 = 5°$, and the initial longitude of the apex of the toroidal ring is at $\phi_0 = 180°$. It can be seen that the loops all show a geometric asymmetry in the inclinations of the two sides of the loop as discussed in Caligari, Moreno-Insertis, & Schüssler (1995, see also Figure 1[b] of Paper II). The angle formed between the tangent vector of the tube and the local horizontal plane (perpendicular to the radial direction) is smaller for the leading side (leading in the direction of rotation) of the loop than the following side. The asymmetry is a consequence of the near conservation of angular momentum as the loop rises, and can explain the observed asymmetric east-west proper motions of the two polarities of an active region during the early stage of its formation (Caligari, Moreno-Insertis, & Schüssler 1995).

The conservation of angular momentum also produces an asymmetry in the tube field strength between the two sides of the emerging loop. As discussed in Papers I and II, the component of the Coriolis force parallel to the flux tube drives a flow of the tube plasma from the leading side of the loop to the following against the direction of rotation. The flow evacuates plasma from the leading leg of the tube and enhances its field strength in comparison to that in the following leg. The numerical simulations of Paper I and II using thermal equilibrium as the initial condition found that the large counter-rotating flow during the rapid rise of the loop produces a significant field strength asymmetry in the final emerging flux loop, with the field strength in the leading leg being significantly greater than that in the following leg at all depths in the convection zone. The stronger field strength in the leading leg will make it more stable against disturbances from convective motions and hence explains the generally better formed, less fragmented leading polarity of an active region in comparison to the following polarity. More recently, the simulations of Caligari, Moreno-Insertis, & Schüssler (1995), using mechanical equilibrium as the initial condition, found that the field strength in the leading tube is not always consistently greater than the following at all levels of the convection zone; for emerging loops with strong initial field strength ($\sim 10^5$ G) the asymmetry reverses in the upper part of the convection zone. Our current simulations begin with non-uniform toroidal flux rings in neutral buoyancy, which

is similar to the initial thermodynamic state used in Caligari, Moreno-Insertis, & Schüssler (1995). The cause for the eruption of the loop is radiative heating rather than the adiabatic growth of the undulational instability of the toroidal flux rings considered in their paper. The results regarding the final field strength asymmetry are illustrated in Figure 9 in which panels (a), (b), and (c) show respectively the variation of field strength as a function of depth along the final emerging loops in panels (a), (b), and (c) of Figure 8. The solid (dash-dotted) lines represent the leading (following) side of the loops. In the case with $B_0 = 30$ kG (panel [a]), the field strength in the leading side is significantly stronger than that in the following side at all levels in the convection zone, consistent with the result in Paper I and II. As $B_0$ increases (panels [b] and [c]), the leading leg field strength is still significantly stronger in the bulk of the convection zone, but they become nearly equal (and even reverse slightly when $B_0$ reaches 100 kG) in the upper layers of the convection zone. This result is similar to what Caligari, Moreno-Insertis, &, Schüssler (1995) found. For smaller values of $B_0$ ($\lesssim 60$ kG), the coherent field strength asymmetry in the final emerging loop suggests that the leading tube should be more stable than the following tube and hence can lead to the formation of an active region with a less fragmented leading polarity than the following. The situation becomes more complex with the final field strength distribution shown in Figure 9(c) obtained for $B_0 = 100$ kG. Further detailed theoretical studies are needed to understand how the field strength distribution along emerging flux loops affects the subsequent formation and morphology of active regions.

## 5. Summary and Discussion

In this paper we modify the energy equation for the model of thin flux tube evolution to incorporate the effect of heat transport by radiative diffusion. Due to the presence of convection, the mean temperature gradient in the convection zone and the overshoot region deviates from that of radiative equilibrium. Therefore there will be a non-zero divergence of radiative heat flux $(dQ/dt)_1$ (see eq. [11]) and this constitutes the main source of heating experienced by a flux tube near the bottom of the convection zone and in the overshoot region. It is important to note that $(dQ/dt)_1$ also applies to every parcel of convecting field-free plasma moving between the top and bottom of the convection zone; it causes a radiative heating near the bottom of the convection zone and a radiative cooling in the surface layers. In addition to $(dQ/dt)_1$, a magnetic flux tube causes changes of the thermodynamic properties within the tube relative to the field free plasma and hence its radiative heating is modified by an additional term $(dQ/dt)_2$. We found that for the flux tube field strengths and magnetic fluxes we consider in the solar interior (those that most likely describe the toroidal flux tubes responsible for active region formation), $(dQ/dt)_2$

is in general much smaller in magnitude than $(dQ/dt)_1$. Since the dominant heating rate $(dQ/dt)_1$ produced by the non-radiative-equilibrium external termperature gradient is only a function of position, the total radiative heating of tube plasma becomes insensitive to the cross sectional radius (and hence $B$ and $\Phi$) of the tube.

As a result of radiative heating, the flux tube rises and eventually erupts to the surface. We find that in the overshoot region, the heating will cause a quasi-static rising of the toroidal flux tubes with an upward drift velocity $\sim 10^{-3}|\delta|^{-1}$ cm s$^{-1}$ which does not depend sensitively on the field strength or magnetic flux of the tubes. In order to store toroidal flux tubes in the overshoot region for a period comparable to the length of the solar cycle, the magnitude of the subadiabaticity $\delta$ ($< 0$) in the overshoot region needs to be as large as $\sim 3\times10^{-4}$. A substantial increase in the magnitude of the subadiabaticity $\delta$ in the overshoot region may be achieved if convective overshooting is considerably reduced by the presence of strong magnetic flux tubes. Furthermore, such a change in the mean temperature gradient towards the direction of radiative equilibrium as a result of the suppression of convective motion would also reduce the radiative heating rate $(dQ/dt)_1$ itself.

Using numerical simulations, we study the formation of emerging magnetic flux loops as a result of radiative heating of the flux tubes. We study the evolution of a non-uniform toroidal flux tube which lies initially at non-uniform depths in the overshoot region and is in a state of neutral buoyancy ($\rho = \rho_e$ at any point along the tube). The apex of the tube is already at the base of the convection zone. We find that radiative heating causes a quasi-static rising of the tube and can bring the upper portion of the tube into a buoyantly unstable state that finally results in the eruption of an anchored flux loop to the surface. Such process is different from the purely adiabatic development of undulational instability of a toroidal tube as considered in e.g. Ferris-Mas & Schüssler (1994), Caligari, Moreno-Insertis, & Schüssler (1995). We find that radiative heating plays an important role in the initial quasi-static development of the rising flux loop near the bottom of the convection zone. Only when the rise of the loop enters the dynamic stage where the growth of buoyancy overpowers the tension and the rise speed is determined by the balance between buoyancy and drag, does the evolution become essentially adiabatic. The fairly short total rise time (2-4 months) obtained from our set of simulations using reasonable initial parameters indicate that radiative heating can be an effective way of causing the eruption of magnetic flux loops that lead to the formation of active regions. The emerging flux loops thus formed show similar qualitative features as were found in previous investigations, e.g. the asymmetries between the leading and following sides of the loop in their latitudes (i.e. the tilt angles), east-west inclination angles, and magnetic field strengths.

Our present calculations have only considered the evolution of the thin magnetic flux

tube *given* the mean temperature stratification of the surrounding field free plasma. The influence of the flux tube on the external fluid is ignored. As we noted earlier, the presence of strong magnetic flux tubes with a sufficiently large filling factor in the fluid can substantially suppress convective motions and hence change the mean temperature stratification of the fluid. This may happen in the overshoot region when strong toroidal flux tubes are being produced by the dynamo process. In the convection zone, however, due to the buoyantly unstable nature of the flux tubes and the background plasma, it is unlikely that this change will take place unless the size of the magnetic structure is sufficiently large ($\gtrsim H_p$). In that case, a local modification of convection and the temperature distribution around the magnetic structure might occur, for example the formation of thermal shadows as described in Parker (1987). The flux tubes we consider have diameters significantly less than the local pressure scale height, hence it is not likely for them to produce substantial modification of the surrounding temperature. It is more likely for the tubes to be heated radiatively and erupt to the surface.

## Acknowledgments

We thank A. N. McClymont, D. W. Longcope, and B. R. Durney for helpful discussions. Y.F. was supported by ONR grant N00014-91-J-1040, and G.H.F. was supported by NASA grant NAGW-3429, NSF grant AST-9218085.

## REFERENCES


Caligari, P., Moreno-Insertis, F., and Schüssler, M.: 1995, *Astrophys. J.* **441**, 886.

Cheng, J.: 1992, *Astron. Astrophys.* **264**, 243.

Choudhuri, A. R.: 1989, *Solar Phys.* **123**, 217.

Choudhuri, A. R. and Gilman, P. A.: 1987, *Astrophys. J.* **316**, 788.

D'Silva, S. and Choudhuri, A. R.: 1993, *Astron. Astrophys.* **272**, 621.

Fan, Y., Fisher, G. H., and DeLuca, E. E.: 1993, *Astrophys. J.* **405**, 390.

Fan, Y., Fisher, G. H., and McClymont, A. N.: 1994, *Astrophys. J.* **436**, 907.

Ferris-Mas, A. and Schüssler, M.: 1994, *Astrophys. J.* **433**, 852.

Howard, R. F.: 1991, *Solar Phys.* **132**, 49.

Mihalas, D.: 1978, *Stellar Atmospheres*, Freeman, San Francisco, pp 185-192.

Moreno-Insertis, F., Schüssler, M., and Ferris-Mas, A.: 1992, *Astron. Astrophys.* **264**, 686.

Parker, E. N.: 1979, *Cosmical Magnetic Fields*, Clarendon Press, Oxford, pp 147-151.

Parker, E. N.: 1987, *Astrophys. J.* **321**, 984.

Shaviv, G. and Salpeter, E. E.: 1973, *Astrophys. J.* **184**, 191

Schmitt, J. H. M. M., Rosner, R., Bohn, H.-U.: 1984, *Astrophys. J.* **282**, 316.

Schüssler, M.: 1978, *Astron. Astrophys.* **71**, 79.

Schwarzschild, M.: 1957, *Structure and Evolution of the Stars*, Dover Publications Inc., New York, pp 62-70.

Spruit, H. C.: 1974, *Solar Phys.* **34**, 277.

Spruit, H. C.: 1981, *Astron. Astrophys.* **98**, 155.

van Ballegooijen, A. A.: 1982, *Astron. Astrophys.* **113**, 99.

## FIGURE CAPTIONS

**Figure 1** - The radiative heating rate $(dQ/dt)_1 = -F_{\rm tot}(d/dr)(\bigtriangledown/\bigtriangledown_{\rm rad})$ as a function of height above the base of the convection zone, computed from Spruit's mixing length model of the solar convection zone (Spruit 1974).

**Figure 2** - The evolution of a non-uniform toroidal ring initially in neutral buoyancy in the overshoot region as described in the text. The initial field strength $B_0 = 60$ kG, total flux $\Phi = 10^{22}$Mx, and the initial latitude $\theta_0 = 5°$. Panel (a) shows the successive positions of the ring in the $r$-$\phi$ plane at time instances $t = 0$, 23, 45, 68, and 83 days. An emerging flux loop is formed and reaches the photosphere after a total time period of 83 days. In comparison, Panel (b) shows the motion of the toroidal ring if the effect of radiative heating is ignored, i.e. assuming adiabatic evolution. The successive positions of the ring in the $r$-$\phi$ plane at uniformly spaced time instances (with an interval of 2 months) are shown. There is small adjustment of the shape of the ring, but over all the ring roughly maintains its initial configuration and precesses in the direction of rotation at the initial angular speed $\omega_0$.

**Figure 3** - The evolution of the conditions at the loop apex for the same case of rising loop discussed in Figure 2. Panel (a) shows the radial position of the loop apex as a function of time. Panel (b) shows the radial accelerations at the loop apex resulting from buoyancy $[(\rho_e - \rho)/\rho]g$ (solid curve), magnetic tension $(B^2/4\pi\rho)(\mathbf{k}\cdot\hat{\mathbf{r}})$ (dashed curve), and the sum of Coriolis and centrifugal forces $-2(\mathbf{\Omega}\times\mathbf{v})\cdot\hat{\mathbf{r}} + v_\phi^2/r$ (dash-dotted curve) as a function of time. The total radial acceleration from the sum of all the forces is also shown (as '+'s).

**Figure 4** - For the same rising loop discussed in Figures 2 and 3, a comparison between the growth of buoyancy at the loop apex resulting from radiative heating $(d\Delta\rho/dt)_{\rm rad}$ (solid line) and that corresponding to adiabatic expansion of tube plasma $(d\Delta\rho/dt)_{\rm ad}$ (dashed line), as a function of the position of the loop apex in the convection zone. The expressions used for computing $(d\Delta\rho/dt)_{\rm rad}$ and $(d\Delta\rho/dt)_{\rm ad}$ are given in the text.

**Figure 5** - The total rise time of the emerging flux loop as a function of the initial field strength $B_0$, for different values of initial latitudes ($\theta_0 = 1°$ ,15° and 30°) and total flux ($\Phi = 10^{21}$ and $10^{22}$ Mx).

**Figure 6** - The emerging latitude of the loops as a function of the initial latitude, resulting from a set of simulations with $B_0 = 30$, 60, and 100 kG, and flux $\Phi = 10^{21}$ and $10^{22}$ Mx.

**Figure 7** - The computed tilt angle of emerging flux loops as a function of the loop emerging latitude obtained from a set of simulations with $B_0$ ranging from 30 to 100 kG, and flux $\Phi = 10^{21}$ and $10^{22}$ Mx. The numbers used as data points indicate the corresponding $B_0$ values in unit of 10 kG ('X's represent $B_0 = 100$ kG).

**Figure 8** - Three examples of the final configuration of the emerging flux loop as viewed from the north pole of the sun. Panels (a), (b), and (c) correspond respectively to the cases with $B_0 = 30$, 60, 100 kG. For all the three cases shown here, the flux $\Phi = 10^{22}$ Mx, the initial latitude $\theta_0 = 5^\circ$, and the initial longitude of the apex of the toroidal ring starts at $\phi_0 = 180^\circ$.

**Figure 9** - The variation of magnetic field strength as a function of depth along the final emerging flux loops in Figure 8. Panels (a), (b), and (c) correspond respectively to the cases with $B_0 = 30, 60, 100$ kG. The flux $\Phi = 10^{22}$ Mx and the initial latitude $\theta_0 = 5^\circ$ are the same for the three cases.

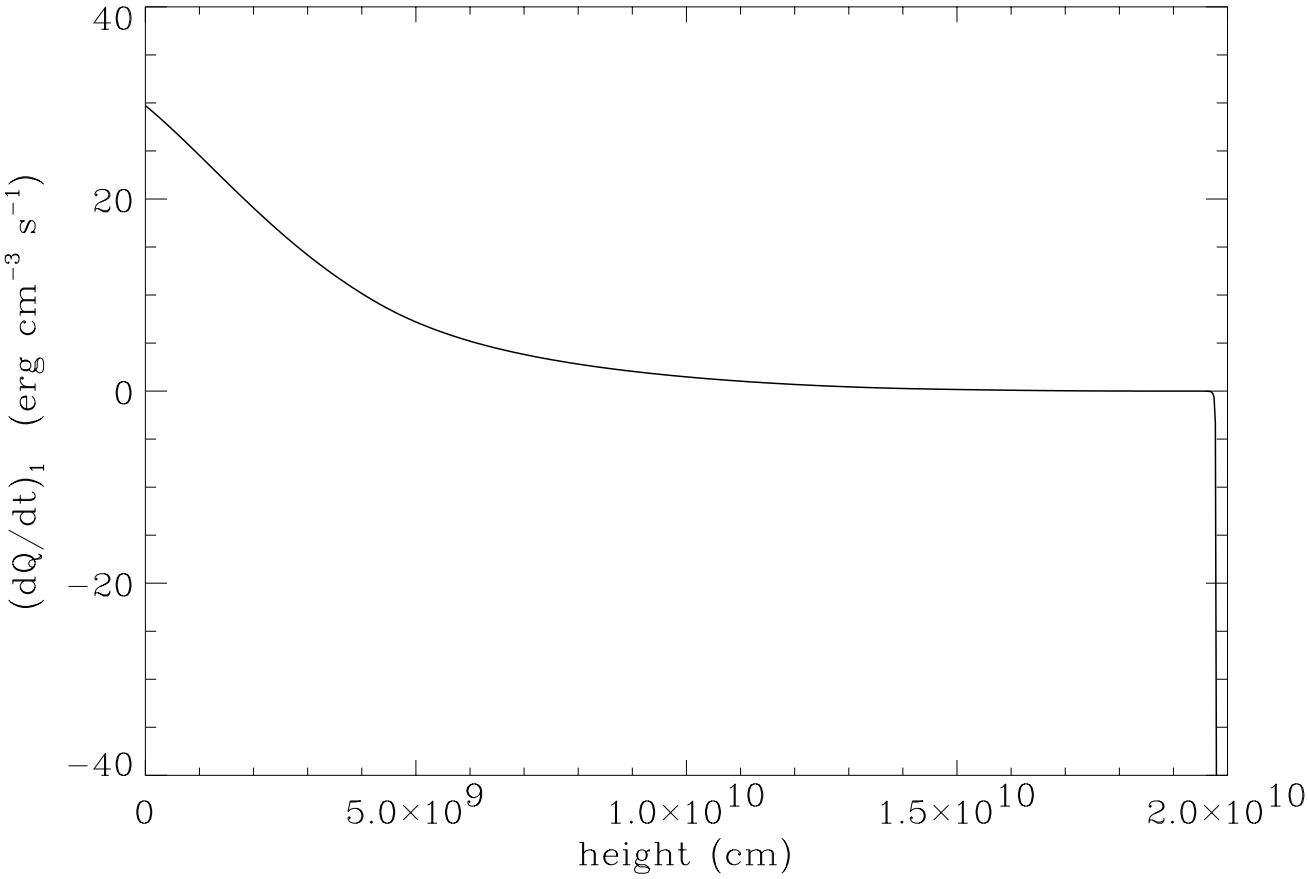
40
20
0
−20
−40
$(dQ/dt)_1$ (erg cm$^{-3}$ s$^{-1}$)
0
5.0×10$^9$
1.0×10$^{10}$
1.5×10$^{10}$
2.0×10$^{10}$
height (cm)

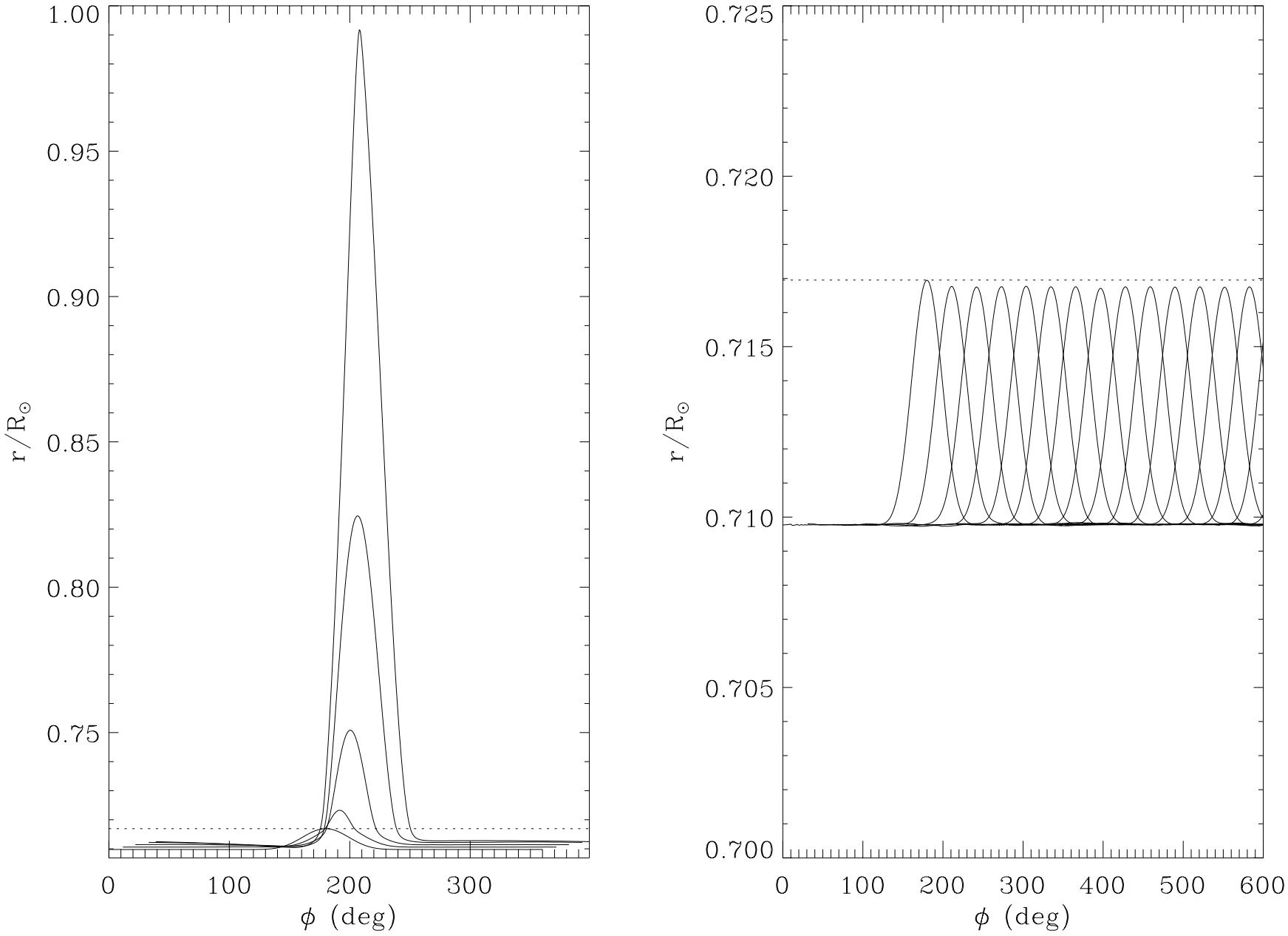
1.00
0.95
0.90
0.85
0.80
0.75
r/R⊙
0
100
200
300
ϕ (deg)
(a)
0.725
0.720
0.715
0.710
0.705
0.700
r/R⊙
0
100
200
300
400
500
600
ϕ (deg)
(b)

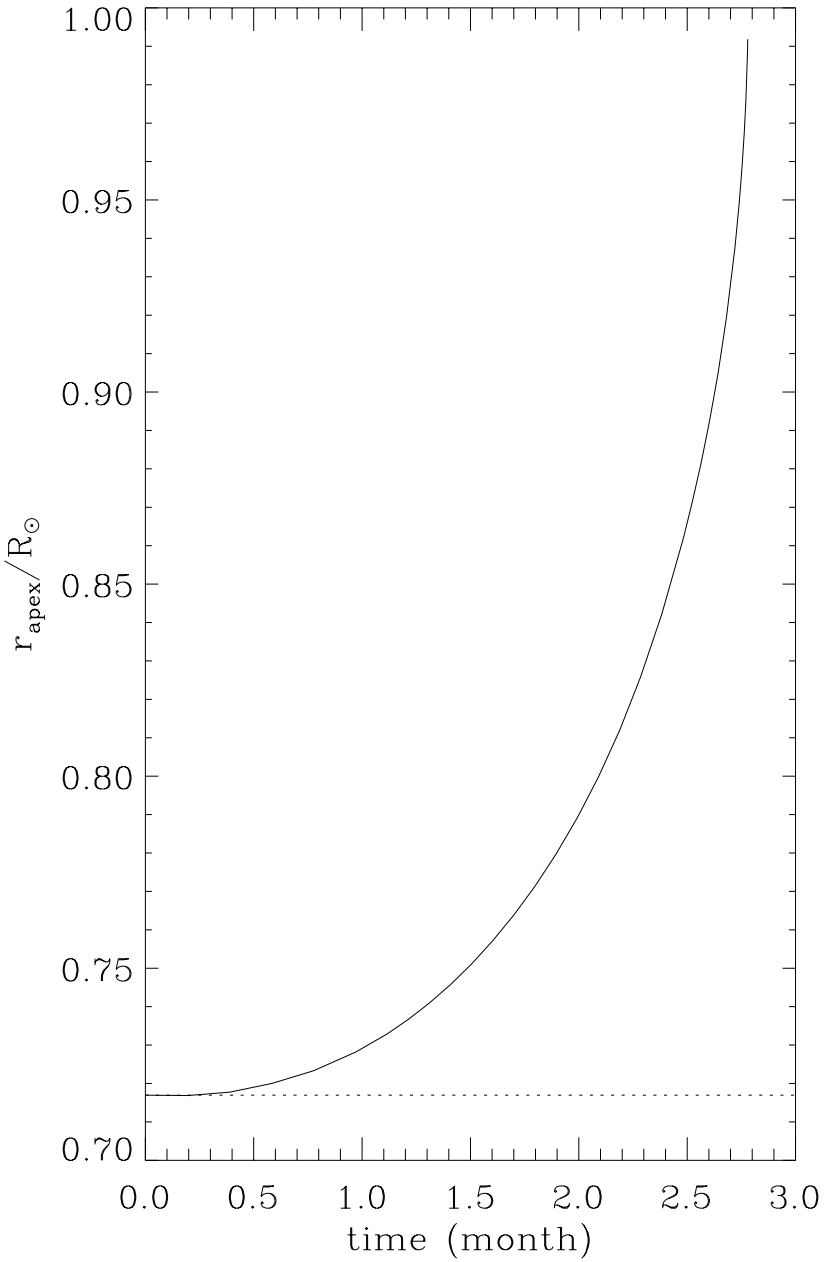
1.00
0.95
0.90
0.85
0.80
0.75
0.70
$r_{apex}/R_\odot$
0.0
0.5
1.0
1.5
2.0
2.5
3.0
time (month)

(a)

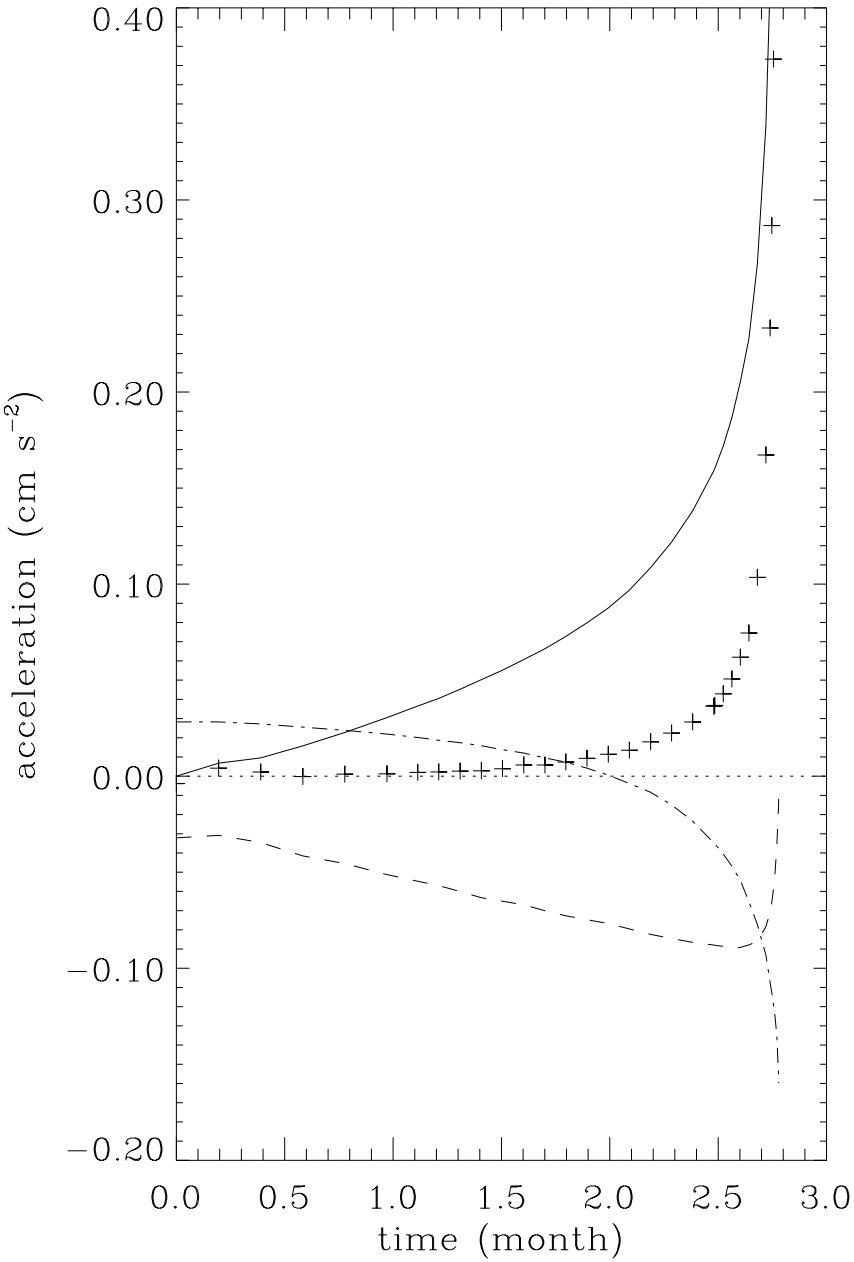
0.40
0.30
0.20
0.10
0.00
−0.10
−0.20
acceleration (cm $s^{-2}$)
0.0
0.5
1.0
1.5
2.0
2.5
3.0
time (month)

(b)

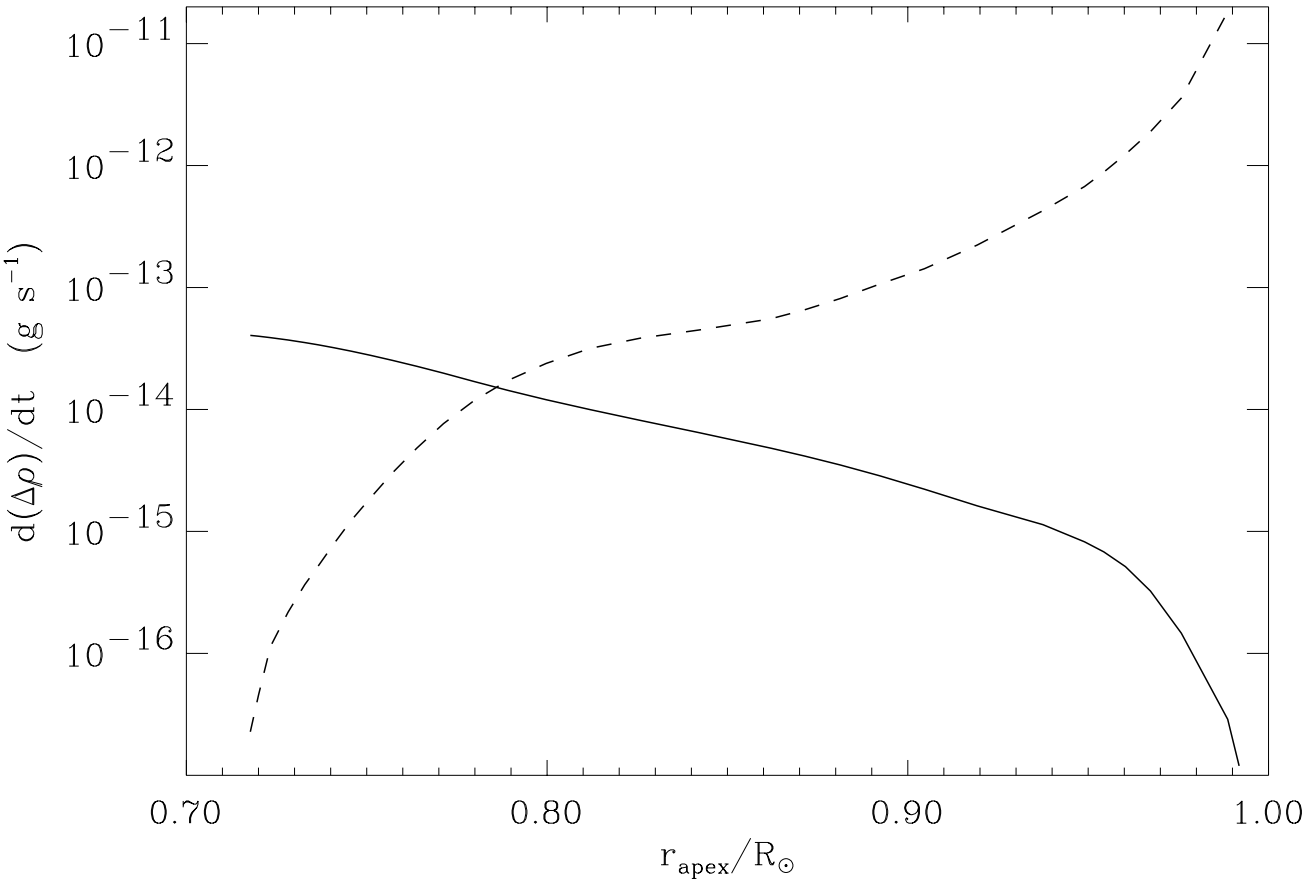
$10^{-11}$
$10^{-12}$
$10^{-13}$
$10^{-14}$
$10^{-15}$
$10^{-16}$
$d(\Delta\rho)/dt$ (g $s^{-1}$)
0.70
0.80
0.90
1.00
$r_{apex}/R_\odot$

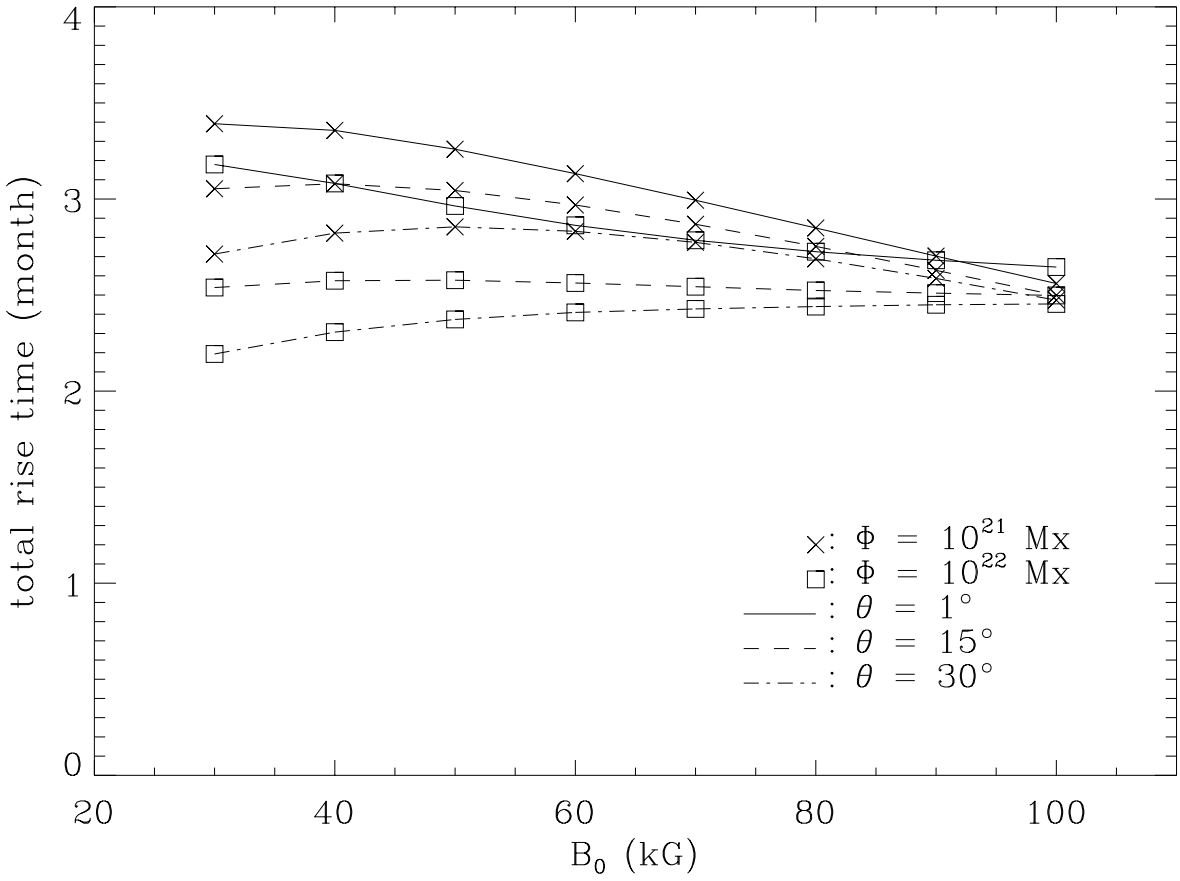
total rise time (month)
B$_0$ (kG)
×: Φ = 10$^{21}$ Mx
□: Φ = 10$^{22}$ Mx
: θ = 1°
: θ = 15°
: θ = 30°
0
1
2
3
4
20
40
60
80
100

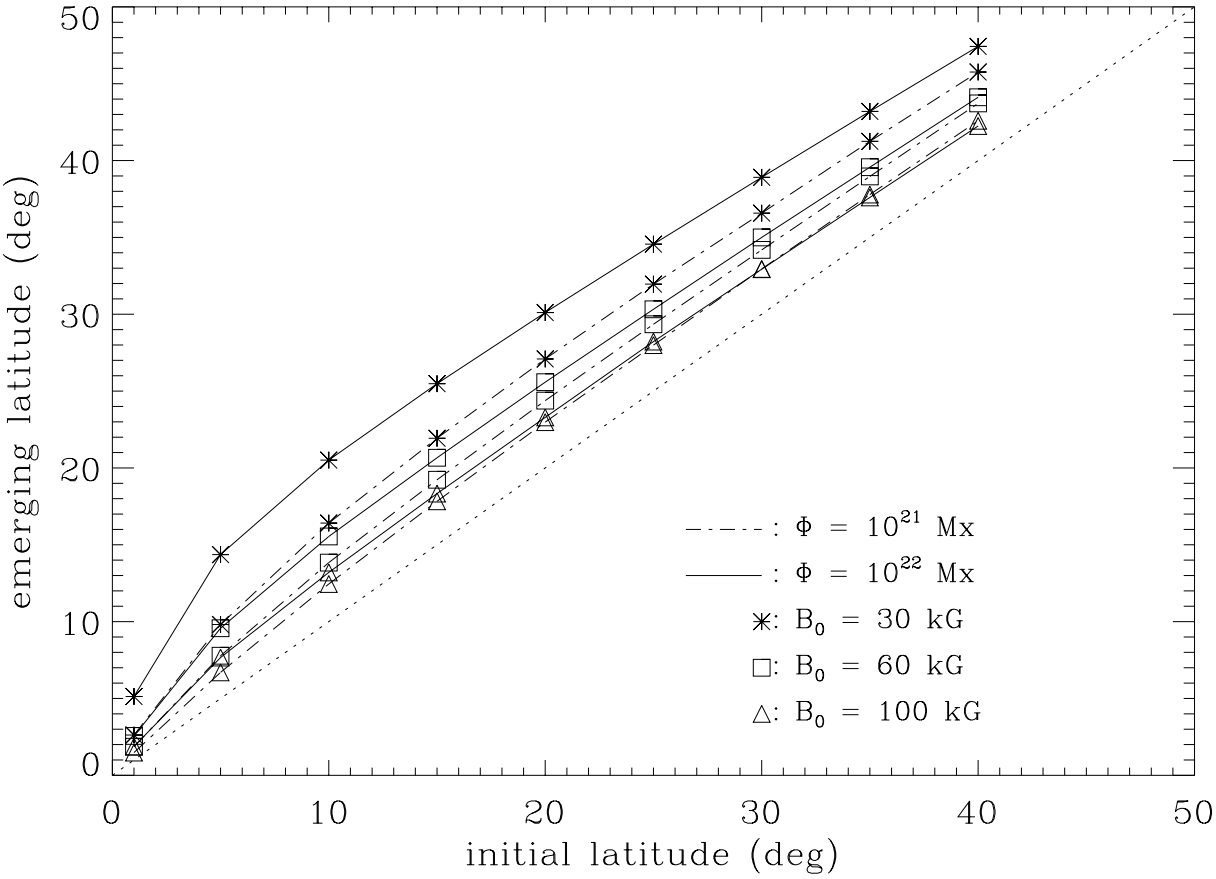
emerging latitude (deg)
initial latitude (deg)
0
10
20
30
40
50
: Φ = 10^21 Mx
: Φ = 10^22 Mx
: B0 = 30 kG
: B0 = 60 kG
: B0 = 100 kG

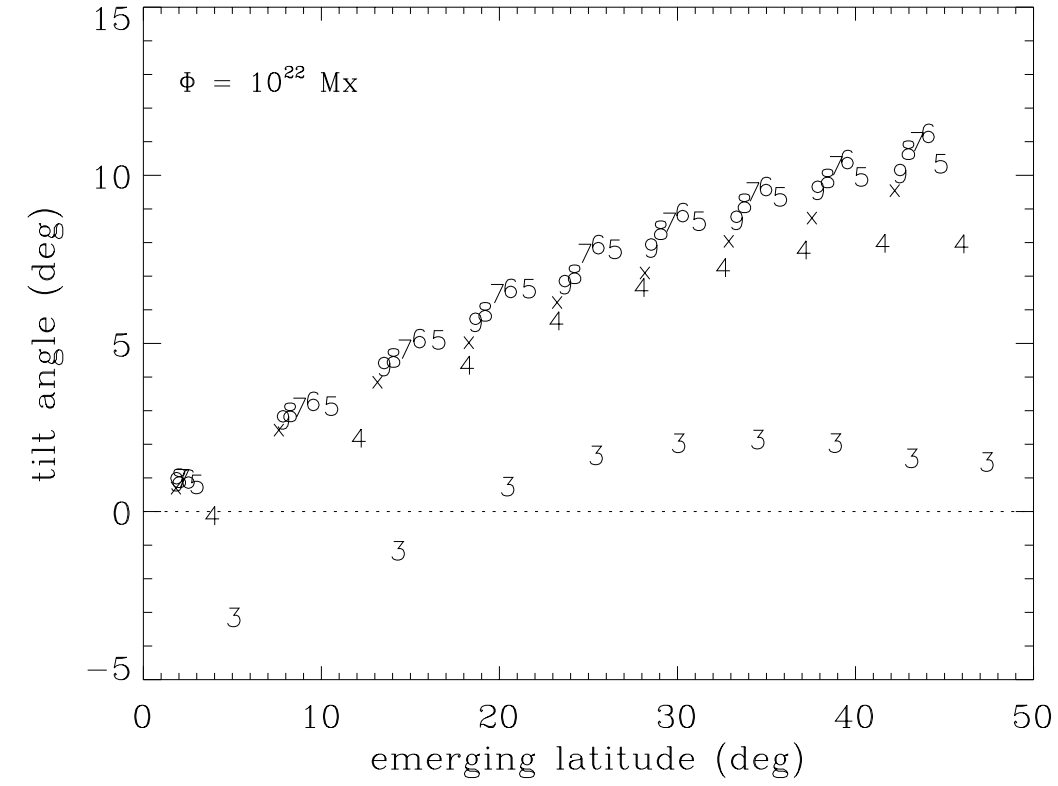
Φ = 10^22 Mx
tilt angle (deg)
emerging latitude (deg)
15
10
5
0
−5
0
10
20
30
40
50

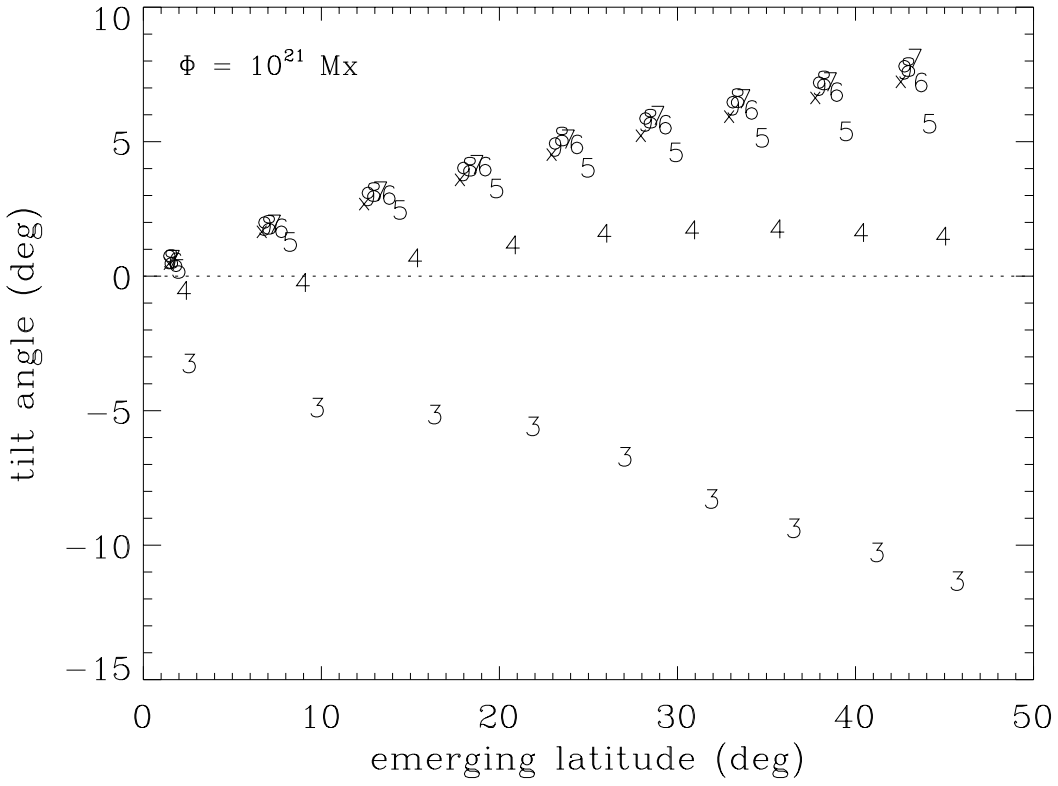
Φ = 10^21 Mx
tilt angle (deg)
emerging latitude (deg)
10
5
0
−5
−10
−15
0
10
20
30
40
50

(a)
(b)
(c)

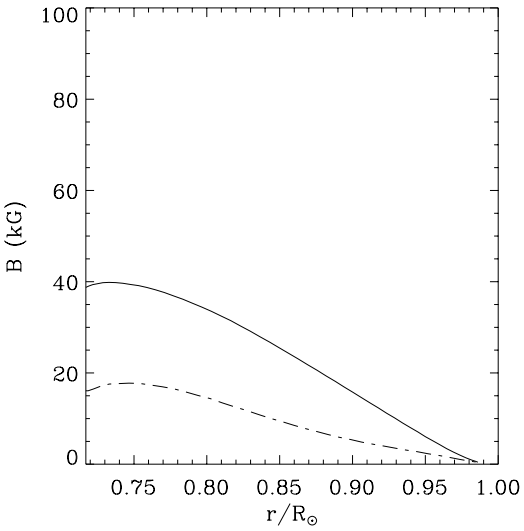
100
80
60
40
20
0
B (kG)
0.75
0.80
0.85
0.90
0.95
1.00
r/R⊙

(a)

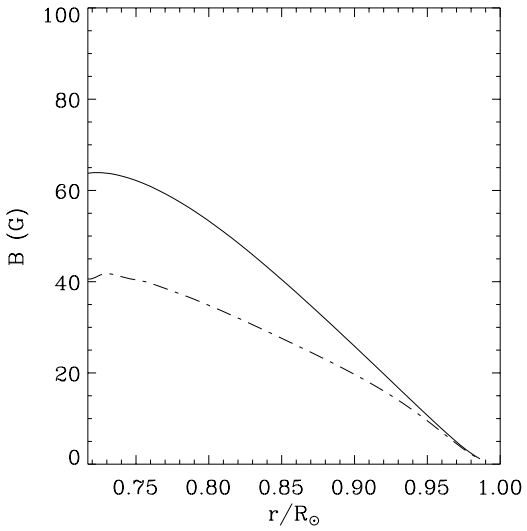
100
80
60
40
20
0
B (G)
0.75
0.80
0.85
0.90
0.95
1.00
r/R⊙

(b)

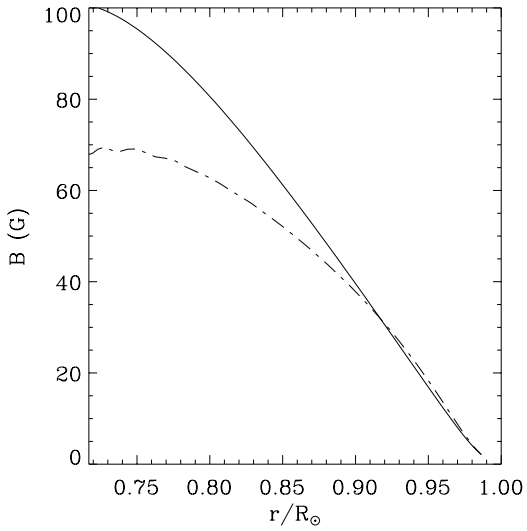
100
80
60
40
20
0
B (G)
0.75
0.80
0.85
0.90
0.95
1.00
r/R⊙

(c)